Spectral and Spatial Characteristic Behaviour of Three-dimensional Radiation Transfer in SF_6 Switching Arcs

S. Esmaeili[1], P. Kloc[2] and J. D. Yan[1]

[1] *University of Liverpool, Department of Electrical Engineering and Electronics*
[2] *Brno University of Technology, Department of Power Electrical Engineering and Electronics*

Abstract
The spectral and spatial characteristics of three-dimensional radiation transfer across an arc column of 0.08 m long, typical in high-voltage gas blast circuit breakers, has been studied in detail. The arc column under study corresponds to an instantaneous current of 15 kA in SF_6 gas at a pressure of 10 bar. Our results show that to calculate the radiative flux divergence (as a volumetric energy source), only a segment of the arc column of 0.024 m in thickness needs to be considered to attain an accuracy of better than 90%. Photons with a frequency lower than 2×10^{15} Hz (150 nm in wavelength) can travel a considerable distance (> 0.02 m) with an intensity attenuation factor of 0.2-0.8. Above 2×10^{15} Hz, only photons from the continuum spectrum can travel up to 0.015 m and line emission is absorbed within a distance of typically 0.0005 m, i.e. the arcing gas is optically thick to these photons.

The arc within a cross-section of the arc column can be divided into a net emission core and a net absorption zone. 55% - 75% of the radiation emitted from the core is reabsorbed in the outer zone. The starting position of the net absorption zone sits within the temperature interval of 75% to 80% of the maximum temperature on the axis. The quantitative information from this work is expected to serve as baseline data for developing improved approximate models for radiation transfer calculation in SF_6 switching arcs.

1. Introduction

Radiation transfer is an effective mechanism to redistribute energy inside and around the conducting core of an arc column. It involves the emission and absorption of photons over a hugely broad spectrum with a frequency between $10^{12} \sim 10^{16}$ Hz, i.e. from short radar waves to long X-rays. Although local thermal equilibrium (LTE) is used to approximate the plasma state of an arc column even at a relatively low current (<600 A) [1, 2], radiation emission from the arcing gas does not obey Planck's law. Because of the abrupt variation of the spectral absorption coefficient as a function of frequency or wavelength (Figure 1), radiation transfer calculation requires the inclusion of every frequency in the above range and spatial integration at every direction in three-dimensional space. Therefore, accurate radiation transfer calculation in industrial systems, such as high voltage gas circuit breakers, is still a prohibitively time-consuming task.

A high voltage gas-blast circuit breaker (HVCB) is a typical example of an industrial arc plasma system and is used to interrupt AC currents, often caused by electrical network fault. In such a device, a transient electrical arc burns in rapidly flowing arcing gas, such as SF_6. The length of the arc column reaches 0.15 m with non-uniform temperature distribution, typically between 300 K and 35,000 K. The gas pressure also varies between 2×10^4 Pa and 6×10^6 Pa (0.2 bar and 60 bar) inside or around the conducting core of the arc where severe ohmic heating maintains the radiation emission at high gas temperature. It is however worth pointing out that the pressure may reach 10^7 Pa or even above, depending on the arcing current. Therefore, radiation transfer calculation in switching arcs requires the spectral absorption coefficient over a wide spectral range and wide temperature and pressure ranges.

SF_6 has a strong global warming effect and its use in high voltage apparatus, especially at extra- and ultra-high voltage levels, is expected to be phased out within the next 10-20 years. Research on SF_6 alternative gases [3, 4] is attracting more interest globally and one of the focuses is on the mechanisms that are responsible for the large differences in interruption performance between SF_6 and other gases with SF_6 serving as the reference for comparison. SF_6 is thus studied in the present work.

The Radiation Transfer Equation (RTE) describes radiation transfer in a medium. In the present work, the medium is a gas. RTE is an integro-differential equation that requires double integration over spectrum and space. Simplified approaches have been developed in the past decades by introducing approximations to particular characteristics of the radiation transfer process to reduce the computational effort.

The P1-approximation is the lowest order of the spherical harmonics method, initially proposed by Jeans in 1917 [5]. It casts an equation for radiation intensity into a set of partial differential equations using

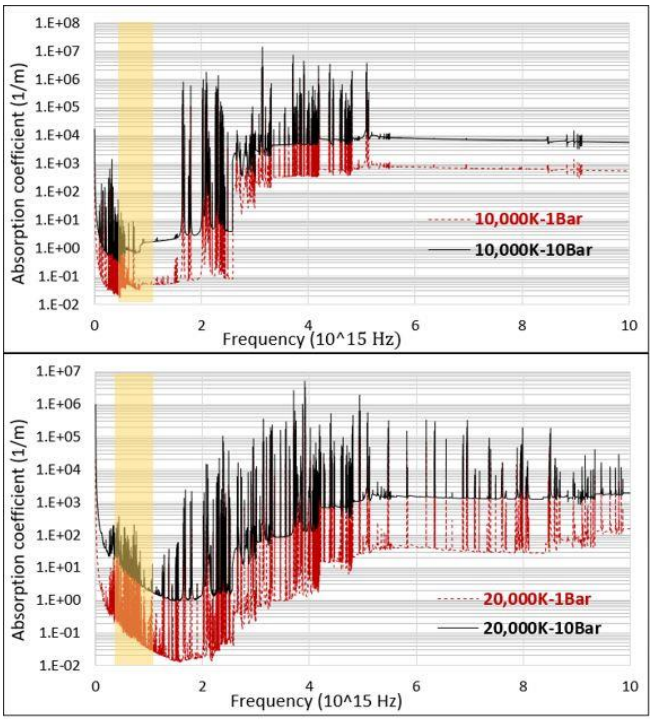

Figure 1. The spectral absorption coefficient of SF6 gas as a function of frequency at different temperatures and pressures. The yellow band is the visible spectrum.

the Fourier series and truncates the set to the lowest order to create a simplified form of the RTE as a function of space only. Although it is not an intrinsic feature of the method, it is a common approach in literature [6, 7] to have more simplifications by dividing the frequency spectrum into a limited number of intervals (bands) and using a mean absorption coefficient (MAC) in each band to simplify the integration over frequency. The MSC can be calculated using one of the averaging methods (Planck, Rosseland, Modified Planck, etc). While being successful for many cases, it may not be reliable when applied to the optically thick regions. It also suffers from accuracy loss at the edge of the arc column where there is a steep temperature gradient [8]. In switching arcs, the accuracy of the calculated radiative flux divergence, at both arc's centre and edge (where strong absorption occurs), will be affected [6, 9]. For example, a comparison between the exact angular solution and P1 approximation, in [6], shows that there is a 12% difference at the arc centre, 17% for the net absorption peak, and up to 48% at the edge of the arc.

The second method is the Partial Characteristic Method (PCM) introduced by Sevastyanenko [10] in 1987. This approach takes advantage of the weak dependence of optical depth on the temperature variation between the two endpoints of a line segment. The calculation of the optical depth is simplified by assuming a linear temperature variation over an integration path. That allows the spectral integration to be carried out independent of the actual temperature distribution, resulting in two characteristic terms, SOM and ΔSim [11, 12], that can be pre-calculated and tabulated. However, its application in switching arc modelling has, so far, been hindered by the extreme gas pressure variation in the arcing space that requires data tables of the partial characteristics for all possible pressure distribution, leading to a situation that cannot be practically handled.

The concept of net emission coefficient (NEC), proposed by Lowke in 1974 [13], has been widely used to consider radiation transfer in thermal plasmas due to its simplicity in the calculation. Typical use is the 1-D empirical model for the fast computation of volumetric radiative energy sources in axisymmetric arcs [14]. This model does not solve the RTE, and its accuracy heavily depends on the definition of the effective emission radius as well as the empirical algorithms to determine the location and size of the net absorption zone [14, 15]. Although the model parameters need to be calibrated by relevant test results, it has been used by circuit breaker manufacturers to aid their product design via arc simulation.

The Discrete Ordinated Method (DOM), initially proposed by Chandrasekhar in 1960 [16], was first applied to radiative heat transfer by Hyde and Truelove in 1977 [17] and more recently by Seegar et al. [18] in arc modelling. The DOM discretises the solid angle into a limited number of regions (numerical quadrature), with each region represented by the RTE in a discrete direction and a weighting factor summing up to 4π for the whole space [19]. The discrete directions need to satisfy the zeroth, first, and second moments [20], and the minimum number required to reach an acceptable accuracy depends on the case geometry. For example, in the present work, trial calculations have shown that 25 directions, in a half-cylinder, provide results of excellent accuracy (99%). This method requires integration over the spectrum and space and is still unacceptable in terms of computation time for the simulation of the arcing process in high voltage circuit breakers.

Other than the approaches discussed above, there are several other solution methods developed for different applications, such as those based on optically thin/thick, proposed by Milne-Eddington, using Schuster-Schwarzschild approximations for 1-D mediums [21], based on the space-volume approximating method of Zonal [22], and the statistical method of Monte Carlo [23]. There is still an ongoing pressing need to develop approximate methods of radiation transfer calculation

for industrial plasma systems targeting rapid computation with acceptable accuracy. The present work is aimed at high-current switching arcs in commercial-scale gas circuit breakers where temperature, pressure and gas composition vary significantly in space and time. The objective of this work is to provide a detailed insight into the radiative characteristics of SF_6 arcs at high currents. Gaining definitive information on the behaviour of radiation transfer in the spectral and space domains and the global and local influences of temperature variations will enable us in future to establish a procedure for the evaluation and development of a rapid radiation transfer calculation model for different arcing devices and gaseous mediums, including environmentally friendly gases that are under heavy research and development effort [3, 24]. The DOM is used to perform the calculation in the present work. The paper is organised as follow. The theory of radiation transfer calculation together with fundamental radiative data is presented in Section 2. A brief comparison with the other researchers' work for result validation is presented in section 3. The selected arc conditions and detailed results are given in Section 4. Concluding remarks are finally made in Section 5.

2. Theory and Method of Calculation

2.1 Basics of radiation transfer

Ignoring the scattering of radiation by particles, radiation transfer for a single frequency (wavelength), at a spatial point, is expressed as [25]:

$$\hat{s}.\nabla I_\upsilon(A,\hat{s}) = K_\upsilon(B_\upsilon - I_\upsilon) \quad (1)$$

for a system in radiation steady-state. $I_\upsilon(A,\hat{s})$ is the spectral radiation intensity that measures the radiative energy flux (per unit area) at point A and in the direction ŝ, with a unit of $[W/(m^2.Hz.sr)]$. K_υ is the spectral absorption coefficient, i.e. the fraction of the intensity absorbed over a unit length of the medium in the direction of radiation propagation. It is a function of temperature and pressure and also varies hugely with frequency. Figure 1 gives an example of its dependence on temperature, pressure and frequency.

B_υ in (1) is the Planck function which describes the emitted spectral energy per unit area and unit solid angle from a blackbody in thermal equilibrium condition [26]. For calculating the intensity at point A, over a line segment AB, with positive direction defined from A to B, the contribution from each point on AB and the incoming intensity, at B, must be taken into account. The total spectral contribution towards A is [6, 27]:

$$I_\upsilon(A) = I_\upsilon(B)\, exp\left(-\int_A^B K_\upsilon(x)dx\right) + \int_A^B B_\upsilon(x)K_\upsilon(x)\exp\left(-\int_A^x K_\upsilon(l)dl\right)dx \quad (2)$$

Where, the first part is the incoming intensity at point B, attenuated along the path AB. The second term (integral part) is the summation of the contributions from the points alongside line AB (from A to B). $B_\upsilon(x)K_\upsilon(x)$ is the spectral emission coefficient at an intermediate point, x. $\int_A^x K_\upsilon(l)dl$ is the optical depth that controls the attenuation of the radiation propagating from x to A. l is a temporary variable whose positive value is the displacement of any point like x from A. Summing the intensities arriving at A from all directions gives the radiation flux vector:

$$F_\upsilon(A) = \int_{4\pi} \hat{s} I_\upsilon(A,\hat{s})d\Omega \quad (3)$$

Integrating the RTE in the form of (2) over the whole solid angle using partial integration gives the divergence of radiation flux which is also the net emission of radiation from a unit volume of the gas at point A:

$$\int_{4\pi}\hat{s}.\nabla I_\upsilon(A,\hat{s})d\Omega = \int_{4\pi}K_\upsilon(A)B_\upsilon(A)d\Omega - \int_{4\pi}K_\upsilon(A)I_\upsilon(A)d\Omega$$

or

$$\nabla.\int_{4\pi}\hat{s}.I_\upsilon(A,\hat{s})d\Omega = 4\pi K_\upsilon(A)B_\upsilon(A) - K_\upsilon(A)\int_{4\pi}I_\upsilon(A)d\Omega$$

or

$$\nabla\cdot F_\upsilon = 4\pi K_\upsilon(A)\left(B_\upsilon(B) - I_\upsilon(B)\right)e^{-\int_A^B K_\upsilon(x)dx} - K_\upsilon\int_{4\pi}d\Omega\int_A^B \frac{dB_\upsilon(x)}{dx}.e^{-\int_A^x K_\upsilon(l)dl}dx \quad (4)$$

In practical radiation transfer calculation, point B is usually in low-temperature gas whose radiation is negligible. There is no significant external radiation entering the arcing space as well. We thus have:

$$\nabla\cdot F_\upsilon = -K_\upsilon\int_{4\pi}d\Omega\int_A^B \frac{dB_\upsilon(x)}{dx}.e^{-\int_A^x K_\upsilon(l)dl}dx \quad (5)$$

The flux divergence per 4π solid angle provides the net emission coefficient (NEC) which, has been extensively discussed in [10].

2.2 Discrete Ordinated Method (DOM)

A cylindrical column of arcing gas is assumed. However, this does not mean the arc column must be straight. The arcing parameters, including temperature and pressure, are obtained from a 2-D axisymmetric

simulation case to make the results relevant to practical switching arc modelling. In the DOM, the 4π solid angle at a target point is divided into ordinate directions, and a partial differential equation is generated to describe the radiation transfer in each ordinate. Thus, integration over the whole 4π solid angle is converted into weighted summation based on numerical quadrature [19]. The contribution from the solid angles are given by the following [14]:

$$\nabla \mathrm{F}_{\upsilon} = K_{\upsilon} \sum_{j=1}^{j=n} \omega_j \left[B_{\upsilon}(0) e^{-\int_0^{x_{wall,j}} K_{\upsilon}(x_j) dx_j} - \int_0^{x_{wall,j}} \left(B_{\upsilon}(x_j) - B_{\upsilon}(0) \right) K_{\upsilon}(x_j) e^{-\int_0^{x_j} K_{\upsilon}(\zeta_j) d\zeta_j} dx_j \right] \quad (6)$$

Where j represents a direction, ω_j is the weighting factor associated with direction j. It is a fraction of the solid angle space. Figure 2 shows a 3-D illustration to consider radiation transfer in one ordinate direction line PW (defined by φ and θ) for a target point P located in a cross-section of the gas column. C is the centre of the cross-section, and the radiative flux divergence is calculated for points like P across the line CG, i.e. from the centre to the edge of the gas column. W is a point on the boundary (represented by x_{wall} in the integration), x_j in (6) represents a point on line PW (such as D), and $B_{\upsilon}(0)$ is the Planck function of the target point P ($x_j = 0$). ζ_j is just an intermediate variable used in the integration. The spectral absorption coefficient, K_{υ}, of SF_6 has been calculated in the temperature range of 300 K to 35,000 K (with a step of 100 K) and frequency range of 10^{12} Hz to 10^{16} Hz (with a step of 2×10^{10} Hz) for different pressures. As explained in section 2.4, the calculations are based on 10,000 frequency points corresponding to a step size of 10^{12} Hz, producing results with sufficient accuracy.

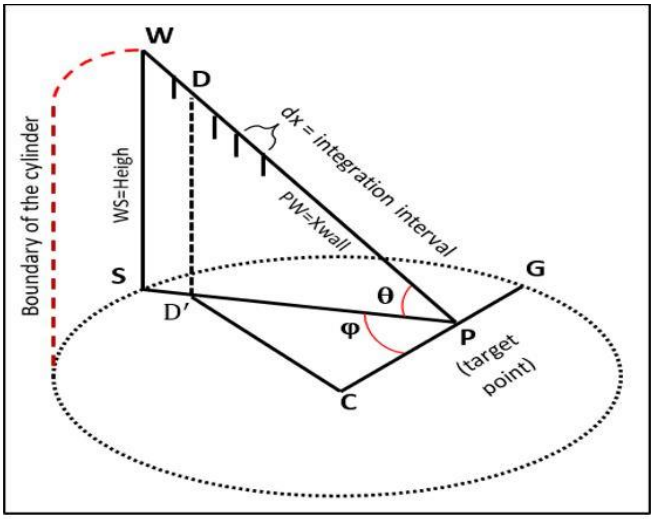

Figure 2. Cross-section of a cylindrical arc

2.3 Temperature profile and inter-dependence between radiation and temperature

Radiation transfer takes place at the speed of light in a gas. The amount of radiative energy emitted or absorbed locally in the arc column depends on the temperature and pressure fields in the arcing space. The shape of the arc column is influenced by the structure as well as the flow field. As shown in Figure 3, at 15 kA before the final current zero in the interruption process of a 245 kV gas blast circuit breaker, gas flowing out from the heating chamber approaches the arc column vertically before it enters the main nozzle and the hollow contact. The arc has the highest axis temperature and the smallest radius of the arc core at

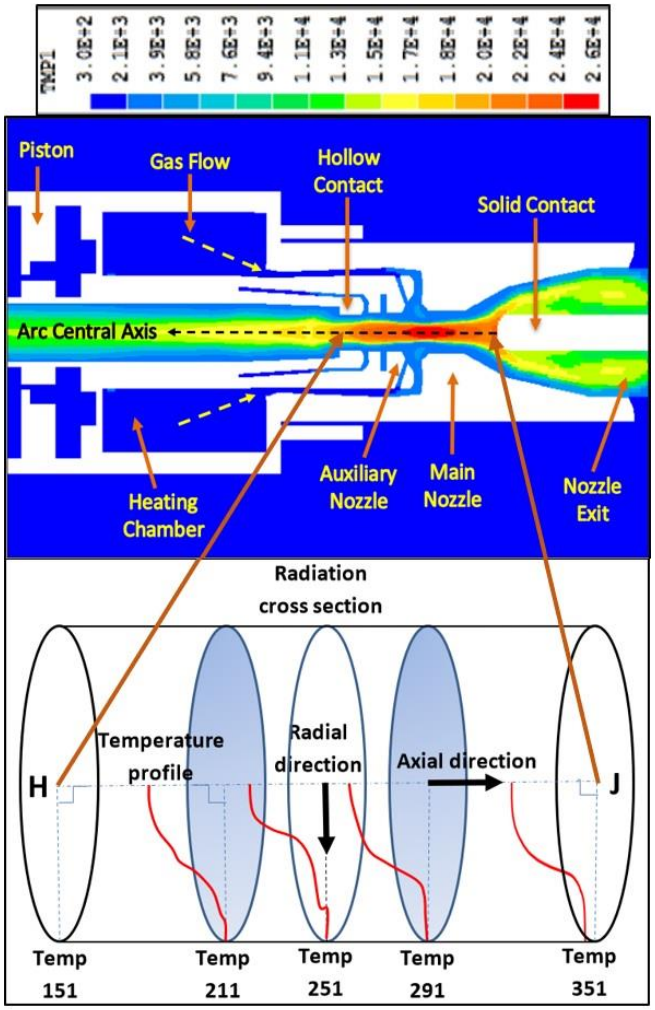

Figure 3. Radial temperature profiles taken from a simulation case of a high voltage circuit breaker. The 0.08 m long arc column used in radiation calculation is constructed from 11 profiles from the same case.

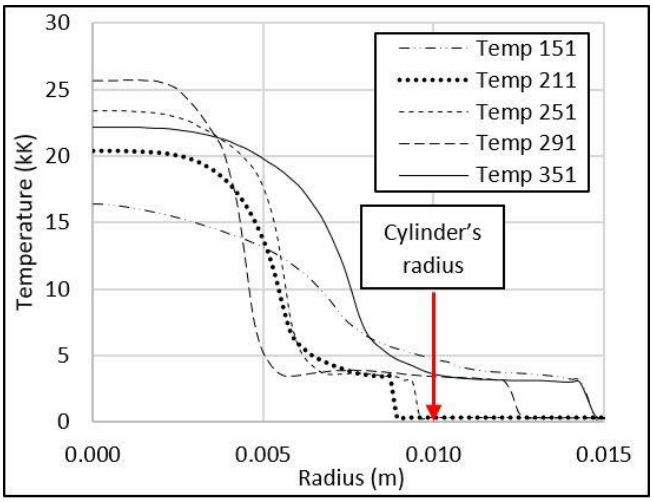

Figure 4. Five radial temperature profiles, chosen at different axial positions in the arc column. The locations of the profiles are indicated in Figure 3. The distance between two consecutive points is assumed to be 0.008 m in simulation. A temperature drop to 0 indicates the nozzle wall.

this location (Profile Temp 251). The axis temperature drops and the arc column broadens slowly when the gas flows towards the exit of the main nozzle and the interior of the hollow contact (see Temp 291 and Temp 211 as examples).

Eleven radial temperature profiles at different axial locations are taken from a transient switching arc simulation where a calibrated 1-D radiation model based on NEC [14] is used. The arc column at this current level is surrounded by a layer of relatively cold gas originating from the high-pressure reservoir (heating chamber). For simplicity, yet without losing the key features of radiation transfer, the pressure is assumed to be uniform at the typical value of 1×10^6 Pa (10 bar). Figures 3 and 4 show four of the eleven radial temperature profiles. The numbers in the profiles' names (Temp 151 or point 151) are the axial position IDs.

The 11 profiles are frozen and then used to construct a 0.08 m long arc column that is to be used in the radiation transfer calculation. This means the actual arc column with a length of 0.16 m is compressed into half of its length. The constructed arc column is in fact a cylinder of constant radius where the arc column occupies most of the space. This is used to represent a situation under challenging flow conditions in reality, i.e. the radial size of the arc column experiences rapid changes in the axial direction of the column. Profile Temp 251 is also located at the centre in the axial direction of the 0.08 m long arc column.

It is worth noting that the constructed arc column of 0.08 m long with 11 variable radial temperature profiles is used in the study presented in section 4, while in this section and section 2.4, arc columns of 0.08 m long but with identical radial temperature profiles at different axial locations are used for ease of interpreting the results.

The first point to note is that our calculation results show that the net radiation emission at the arc centre responds well to the local temperature change (Figure 5). The objective is to gain a quantitative understanding of the sensitivity of net radiation emission (the radiation flux divergence) to the overall change in gas temperature. Radiation transfer calculation is carried out in 3-D space based on equation (6) with 25 directions for a half-cylinder. For a 0.08 m long column with identical radial temperature profiles at different axial locations, increasing the radial temperature profile by 1% (1% of local temperature at each point) leads to a 3.5% increase in the flux divergence on the axis (centre) of the middle cross-section of the column and 4.4% in the net absorption peak (near the edge of the arc column). A 5% increase in temperature produces 18% and 19% increases, respectively, at the arc centre and for the net absorption peak. In the reference case in Figure 5, 60% of the radiative flux emitted from the net emission core is re-absorbed in the net absorption zone.

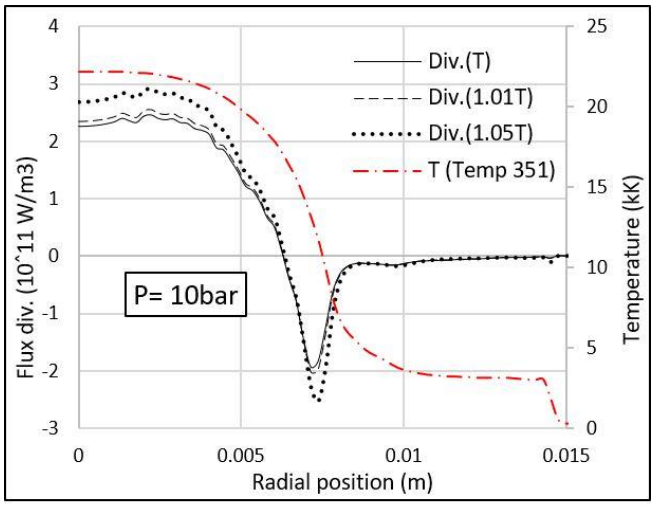

Figure 5. Flux divergence of SF6 in the middle plane of a 0.08 m long column with identical radial temperature profile. For 2 of the cases, the radial temperature profile has been increased by 1% and 5%.

2.4 Minimum required number of directions and wavelengths data points

The number of coordinate directions in space, the number of wavelength points over the spectrum in the absorption coefficient data table, and the dominant frequency spectra are three crucial factors that affect the

accuracy of radiative flux divergence calculation. In this section, we investigate these factors to find an optimum number for each one to make a trade-off between the accuracy and the computation time.

To verify the dominant frequency spectra, the spectrum between 10^{12} and 10^{16} Hz has been divided into 20 equal bands (Table 1), and the flux divergence is calculated for each one as well as the entire spectrum. The results are calculated for four cases. The first three cases (shown in Figures 6a, 6b, and 6c) are with axially-identical temperature profiles, corresponding to the three profiles in Figure 4 (Temp 351, 291, and 151). Here, the target cross-section is at the middle of the 0.08 m long arc column. The fourth case (shown in Figure 6d) is with variable temperature profiles, containing 11 profiles across the cylindrical space. The temperature profile at the centre in the axial direction (the target cross-section) is Temp 251 in Figure 4.

Figures 6 and 7 present detailed results on the

Table 1 – Frequency bands ($\times 10^{15}$Hz)

Band	1	2	3	4	5
From	0.00100	0.50102	1.00104	1.50106	2.00108
To	0.50100	1.00102	1.50104	2.00106	2.50108
Band	6	7	8	9	10
From	2.50110	3.00112	3.50114	4.00116	4.50118
To	3.00110	3.50112	4.00114	4.50116	5.00118
Band	11	12	13	14	15
From	5.00120	5.50122	6.00124	6.50126	7.00128
To	5.50120	6.00122	6.50124	7.00126	7.50128
Band	16	17	18	19	20
From	7.50130	8.00132	8.50134	9.00136	9.50138
To	8.00130	8.50132	9.00134	9.50136	10.0

contribution of different bands to the radiation flux divergence at several radial points at the middle plane of the arc column. Each curve is made of 20 values, representing the contribution from 20 bands at a given point. The first point of each case is the centre of the relevant cross-section with the highest temperature. The main points from the results are:

1) The frequency upper limit for considerable emission and absorption has a clear dependence on the maximum temperature. The cut-off frequency band is 13 at 25,000 K (Temp 291), 12 at 23,000 K (Temp 251), and 9 at 16,000 K (Temp 151).
2) Negligible effect for net absorption of radiation from bands 1-3 and 13-20.
3) Counting only the contributions from the first 11 bands (from 10^{12} Hz to 5.5×10^{15} Hz) is sufficient to achieve a calculation accuracy of more than 95% for net absorption and more than 97% for the net emission in the arc core.
4) Radiation absorption starts at $T = 0.75T_{max}$ (after the red line in Figure 7). Although for most of the profiles $T \simeq 0.8T_{max}$ can be determined the

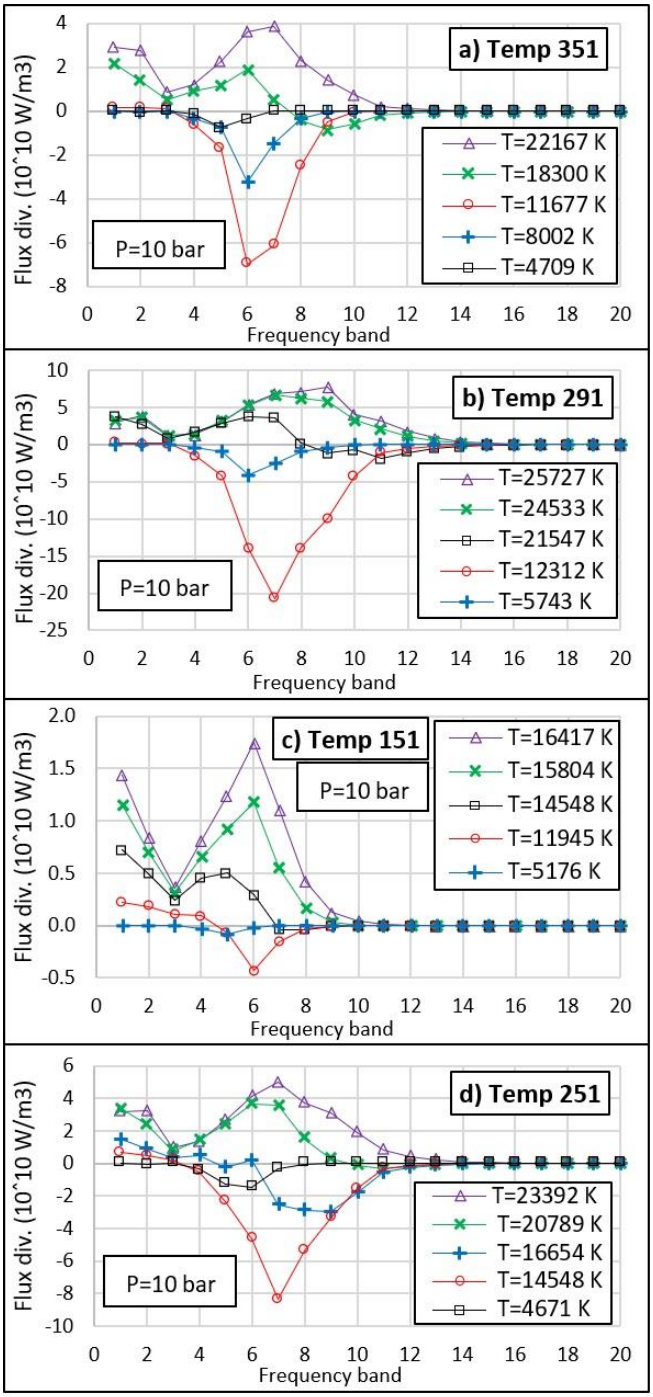

Figure 6. Divergence of radiation flux contributed by each band (horizontal axis) at 5 radial positions where the arc temperatures are different. a) Temp 351 and the whole cylinder follows the same radial temperature profile, b) Temp 291 with the same assumption as in a, c) Temp 151 with the same assumption as in a, d) Temp 251 with all 11 temperature profiles used in the calculation.

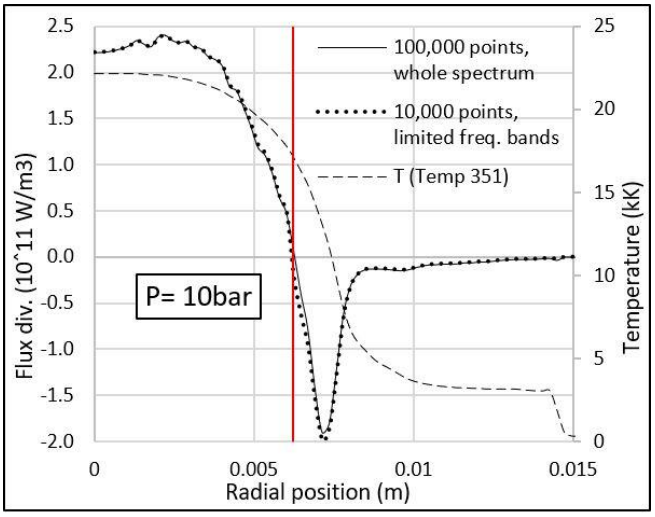

Figure 7. The flux divergence of SF_6 with different frequency intervals; 25 directions in half-cylinder. Red line indicates the dividing point between emission and absorption zones.

border between two regions, $0.75T_{max}$ is considered a safe margin to use fewer bands for radiation absorption calculation.

The rate of change of the absorption coefficient against frequency becomes lower when the temperature is higher than 12,000 K. This means it is possible to use a larger frequency interval for the arc region where T>12,000 K.

To determine the largest frequency step size for integration, two sets of calculations are performed for a temperature profile close to point J in Figure 3 (Temp 351): first with 100,000 frequency points equally distributed from 10^{12} to 10^{16} Hz corresponding to a frequency interval of 10^{11} Hz, and another one with only 10,000 points and an interval of 10^{12} Hz. For the latter, a limited number of frequency bands have been chosen to test the conclusions 2, 3, and 4 above. It contains bands 1 to 11 for $T > 0.75T_{max}$ and bands 4 to 11 for $T < 0.75T_{max}$. Results are displayed in Figure 7. The difference between the two sets of results is less than 1% at the centre of the arc and less than 5% at the absorption peak; however, it leads to a computing time reduction of 94% based on a single-core, reducing from 947 s to just 60 s per spatial point on a desktop computer with Intel(R) Core(TM) i5-4570T 2.90GHz.

The influence of the number of directions is shown in Figure 8 for Temp 351 in Figure 3. Due to geometrical symmetry (axisymmetry), the calculation only needs to be performed for half of the target cross-section (0 to 180 degrees) to obtain the radiative flux divergence. The number of directions refers to the calculation for this half cross-section. The difference between 25 and 234 directions is negligible. In terms of the total radiative energy escaping from the arcing gas (cylinder of the radius of 0.015 m), the error is merely 1%. Therefore, 25 directions are used for the calculation in the rest of the work.

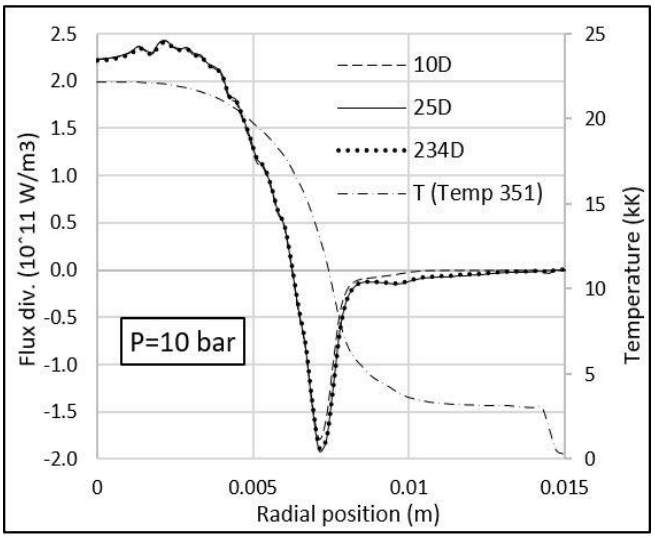

Figure 8. Radiation flux divergence using different DOM directions for radial temperature profile Temp 351.

Results on frequency step size and the number of directions for spectral and spatial integration were also obtained for other profiles. They are very similar to those on Temp 351 and thus will not be repeated.

3. Validation of the Model

No reliable experimental results exist, for verification of radiation transfer calculation of thermal plasmas, where experimental conditions are fully specified. One common approach is to compare with published work.

The radiative flux divergence has been calculated based on two temperature profiles from the literature, and results are compared with previously published results. The first one, presented in Figure 9, is based on the temperature profile used by Randrianandraina et al. [7] and, the second one, given in Figure 10, is based on the Tiemann temperature profile [28] used by Nordborg and Iordanidis [6]. The work in [6] and [7] is based on the DOM in a cylindrical space. The number of directions in [6] is 45 for the whole solid angle which is close to our number (25 in the half-cylinder or 50 in the whole solid angle). In [7], between 8 and 72 directions are applied with insignificant differences between their results. The number of frequency points is much higher than the present work (300,000). However, as shown in Figure 7, using more than 10,000 frequency points leads to a little improvement in the results.

Results from the present work compare well with results obtained in [6, 7] but with noticeable

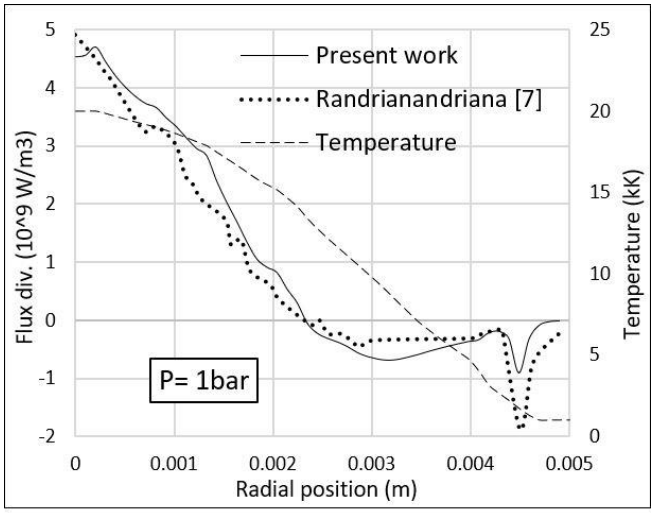

Figure 9. Radiative flux divergence in a 2-D model based on the profile from Randrianandraina, et al [7].

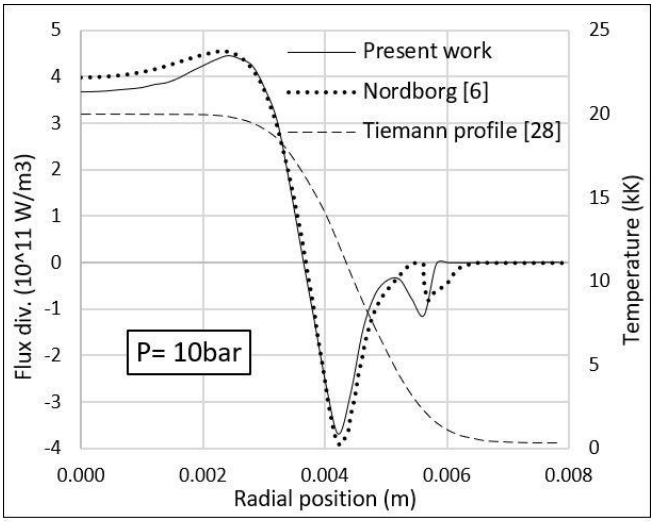

Figure 10. Flux divergence based on Tiemann profile [28]; comparison with Nordborg and Iordanidis work [6]

differences. It is our opinion that the differences are mainly caused by the input data of spectral absorption coefficient; which, is a function of frequency, temperature, and pressure. For completeness, Figure 11 presents some samples of the spectral absorption coefficient used in [6, 7] for comparison with the present work's data. The difference between the data used by Nordborg and Iordanidis [6] and in the present work (Figure 11a) is clear. In the case of Randrianandraina et al. [7], although their input data is similar to ours (Figure 11b), there are significant differences. For example, over the frequency band between 1×10^{15}Hz and 2×10^{15}Hz, the density and magnitude of the absorption lines' peaks in the data used in this work are higher. But at the vicinity of 3.5×10^{15}Hz, it is an opposite comparison. In the two cases shown in Figures 9 and 10, 74% and 60% of the radiative flux emitted from the net emission core is re-absorbed in the net absorption zone, respectively.

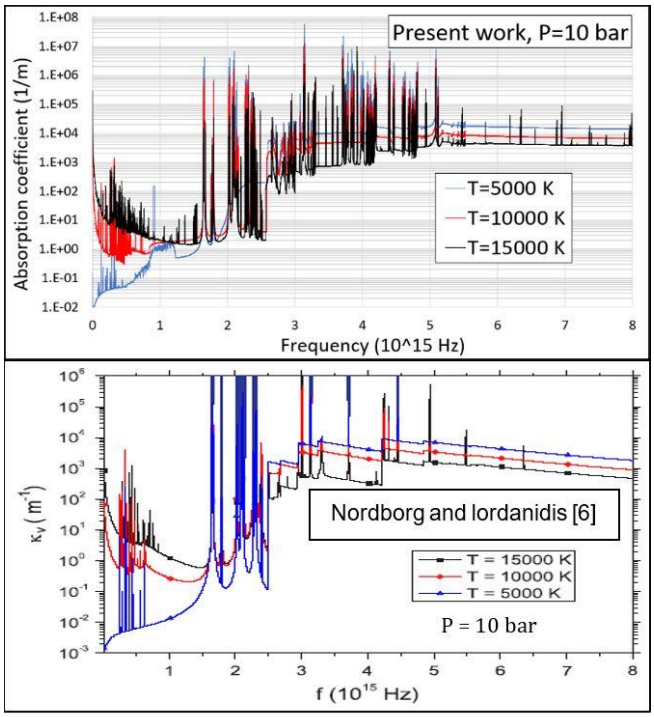

Figure 11a. Absorption coefficient spectrum of the present work and Nordborg and Iordanidis [6]

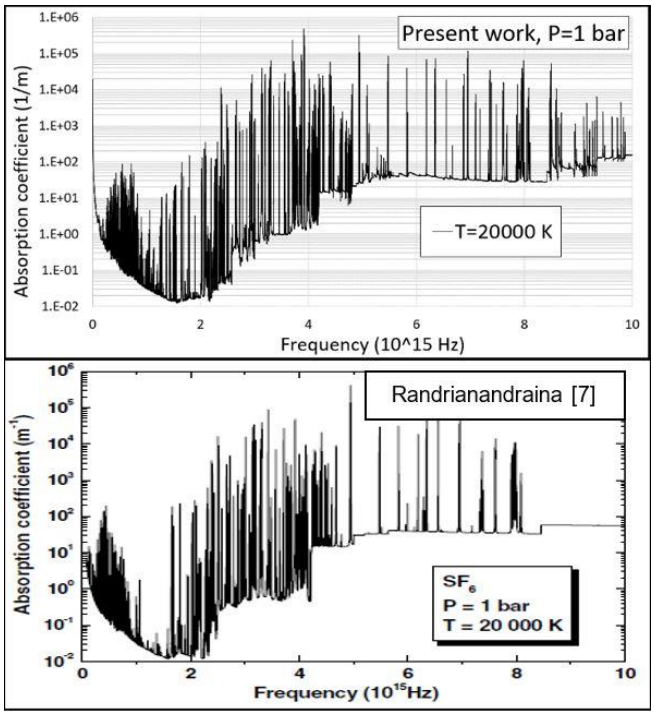

Figure 11b. Absorption coefficient spectrum of the present work and Randrianandraina, et al [7]

4. Results and analyses

4.1 Temperature distribution used in radiation transfer calculation and overall behaviour

As stated in Section 2.3, 11 temperature profiles from the circuit breaker arc simulation have been used to construct a 0.08 m long column of gas to represent a

situation with sufficient complexity for radiation transfer. The axis temperature difference between two adjacent radial profiles is less than 10%. Temperatures on all intermediate points are obtained by interpolation.

The radiative flux divergence along the radius in the target cross-section has been calculated for seven selected cases (Table 2) which differ in the length of the arc column included in the calculation and the location of the target cross-section. These cases are selected to study the radiation transfer characteristics of practical switching arcs. The target cross-sections are all located at the middle of each selected column that may differ in their length. Three cases, A, B and C, were chosen to represent the different parts of the arc column.

Table 2- Different case studies. Z=0 is the cross-section of point J in Figure 3 with profile Temp 351 (Figure 4) and Z=0.08 m is the cross-section of point H in Figure 3 with profile Temp 151

Case	Description
A1	The whole cylinder (0.08m) with 11 temperature profiles. Target points are at the middle of the cylinder (Z=0.04 m; point 251, Figure 3)
A2	A short segment of the cylinder with the length of 0.032 m (5 temperature profiles). Target points are the same as A1.
A3	A short segment of the cylinder with the length of 0.024 m (3 temperature profiles). Target points are the same as A1.
B1	Half of the whole cylinder close to point J with 6 temperature profiles; length is 0.04 m and radiation cross section is located at the middle of the section.
B2	Central part of the case B1 with the length of 0.024 m (4 temperature profiles). Target points are the same as B1.
C1	Half of the whole cylinder close to point H with 6 temperature profiles; length is 0.04 m and radiation cross section is located at the middle of the section.
C2	Central part of the case C1 with the length of 0.024 m (4 temperature profiles). Target points are the same as C1.

Figure 12a presents the differences in the radiative flux divergence for cases A1, B1 and C1 with their radial temperature profiles given in Figure 12b.

The radiative flux divergence represents the difference between the emitted radiation from a unit volume of the

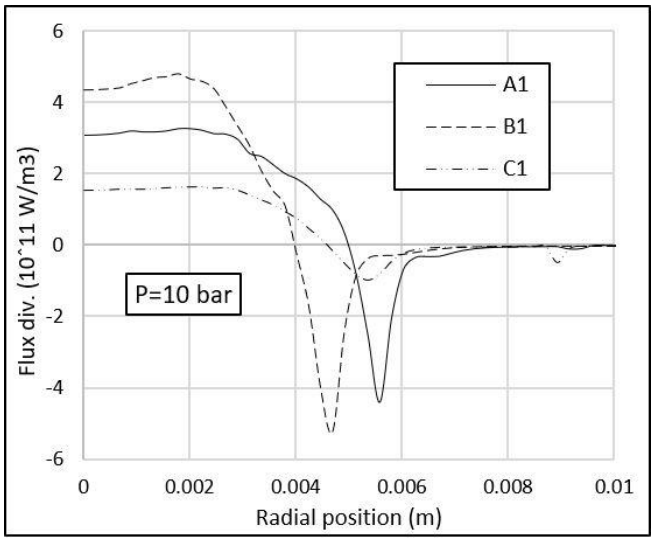

Figure 12a. Radiative flux divergence at the middle cross section of three selected lengths of the arc column

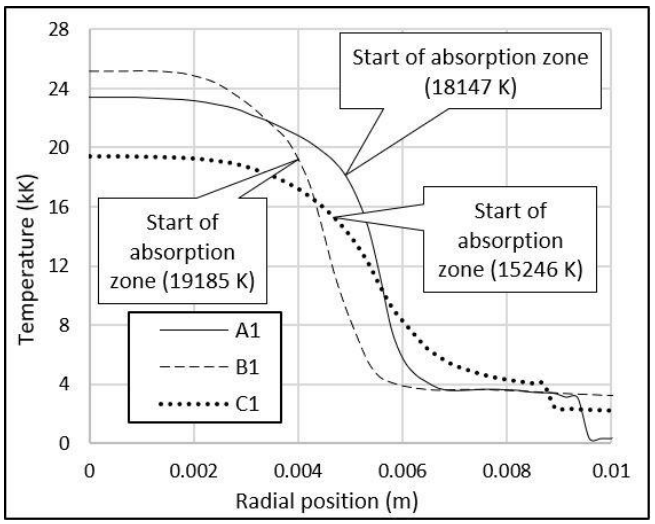

Figure 12b. Radial temperature profiles in the target cross-sections of cases A1, B1 and C1.

gas and the absorbed radiation passing the unit volume from all directions. The flat temperature variation at the centre of the arc leads to an increasing radiative flux divergence [6] in the first 0.002 m, most apparently in case B1 (Figure 12a). Results of radiative flux divergence for an isothermal sphere also clearly shows this phenomenon for points away from the centre. That is an important point to note; because it explains why the outmost layer of an initially isothermal plasma sphere will become cooled first when convection and thermal conduction are negligible due to the increased power loss from the edge.

Radiation absorption at a point depends on the local absorption coefficient and the arriving radiation intensity for a given frequency (equation (1)). The arc core usually has the highest temperature, and it emits many more photons at higher frequencies [12], see

Figure 1 and Figure 6b. Figure 6b clearly shows that when the arc temperature decreases at the arc edge, photons of the highest frequency (bands 10-15) are first absorbed by the immediately surrounding colder layer (T=21547 K), followed by powerful absorption of photons in bands 5-10 at T=12312 K. The low-temperature gas in the surrounding region (T=5743 K) only absorbs photons in bands 5-8. The peak absorption frequency reduces over the slope of the arc's edge when the temperature goes down.

It is to be noted that a pocket of gas, such as that at T=21547 K in Figure 6b, absorbs photons from the arc centre in bands 8-15 but emits lower frequency photons (bands 1-8), depending on its relative position in the temperature profile. Its overall radiative behaviour will be the sum of the contributions from all the bands. Radiation absorption in SF_6 is more effective in wavelengths less than 130 nm (frequency > 2.3×10^{15} Hz) at low temperatures [7, 12], as can be seen in Figure 1.

Due to the relatively low temperature at the arc centre, radiation in case C is at the lowest level (Figure 12a). Despite the differences in the temperature profiles and the arc centre temperatures, the net absorption peak always takes place at the middle of the slope, corresponding to a temperature around 11,000 K.

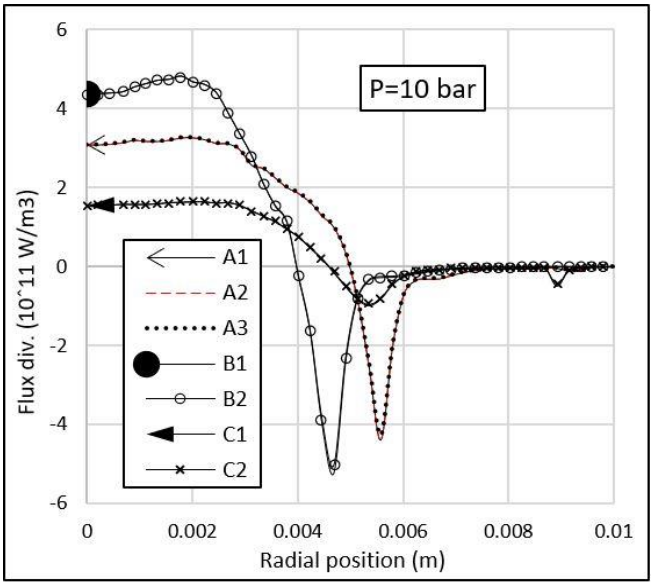

Figure 13. Flux divergence at different cross-sections of the cylinders with different lengths

Figure 13 displays the radiative flux divergence distribution in the radial direction for all 7 cases listed in Table 2. The first and most apparent feature is that, for practical SF_6 switching arcs, radiation transfer as an energy transport mechanism is mostly determined by the radial temperature profile in the target cross-section. A thickness of 0.012 m on each side of the target cross-section is sufficient to achieve an accuracy of better than 90%.

4.2 Spectral characteristics along typical optical paths in the selected arc column

Radiation transfer in an arcing gas involves the emission and absorption of photons at different frequencies. In the present work, a very large spectrum is considered. Photons of different nature (line or continuum) at different frequencies behave differently over a spatial optical path. The whole spectrum is divided into 20 bands and for each band, a representative emission line and a representative frequency for the continuum are chosen to elucidate their differences in the emission and absorption behaviour. To be quantitative, the attenuation coefficient, as defined by the term $e^{-\int_0^x K_\upsilon dl}$ in equation (6), has been calculated for the selected lines and continuum. The division of the bands is given in Table 1 and the selected frequencies are given in Table 3. Figure 14 displays the attenuation over three typical paths from an arbitrarily selected target point P (Figure 14a) to the edges of a cylinder. For comparison, the spectral line is chosen to be closest to the continuum frequency.

Table 3 - Line and continuum frequencies

Band	from freq. (Hz)	to freq. (Hz)	line (Hz)	continuum (Hz)
1	1.00000E+12	5.01000E+14	3.25320E+14	3.51000E+14
2	5.01020E+14	1.00102E+15	7.20840E+14	7.16240E+14
3	1.00104E+15	1.50104E+15	1.22974E+15	1.23102E+15
4	1.50106E+15	2.00106E+15	1.79872E+15	1.84100E+15
5	2.00108E+15	2.50108E+15	2.31382E+15	2.32676E+15
6	2.50110E+15	3.00110E+15	2.95532E+15	2.96662E+15
7	3.00112E+15	3.50112E+15	3.14950E+15	3.15502E+15
8	3.50114E+15	4.00114E+15	3.71594E+15	3.72100E+15
9	4.00116E+15	4.50116E+15	4.20458E+15	4.21496E+15
10	4.50118E+15	5.00118E+15	4.63166E+15	4.63578E+15
11	5.00120E+15	5.50120E+15	5.12642E+15	5.13106E+15
12	5.50122E+15	6.00122E+15	5.82210E+15	5.80000E+15
13	6.00124E+15	6.50124E+15	6.33816E+15	6.30000E+15
14	6.50126E+15	7.00126E+15	6.88210E+15	6.90000E+15
15	7.00128E+15	7.50128E+15	7.35836E+15	7.35000E+15
16	7.50130E+15	8.00130E+15	7.88798E+15	7.83970E+15
17	8.00132E+15	8.50132E+15	8.08284E+15	8.15970E+15
18	8.50134E+15	9.00134E+15	8.51302E+15	8.55970E+15
19	9.00136E+15	9.50136E+15	9.10112E+15	9.40000E+15
20	9.50138E+15	1.00000E+16	9.78928E+15	9.78240E+15

For comparison, the spectral line is chosen to be closest to the continuum frequency. The important information from the results is summarised below:

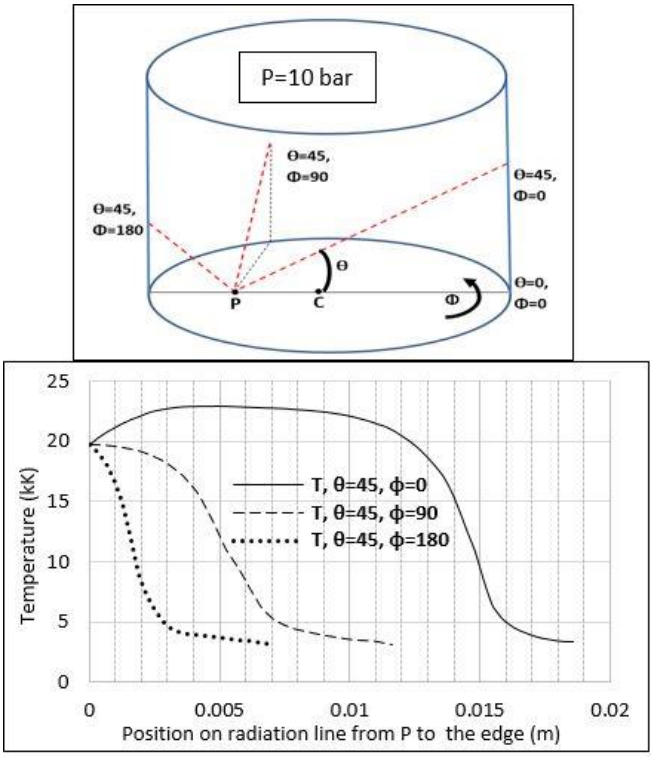

Figure 14a. Three radiation paths from the target point P=0.00446 m and their temperature profiles

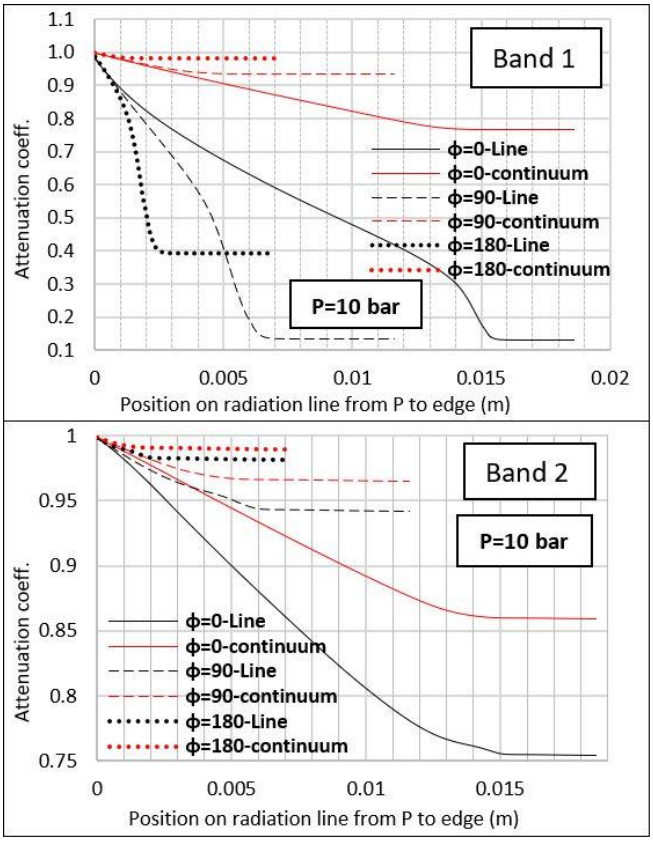

Figure 14b. Attenuation of 3 paths in Figure 14a in some typical frequencies of bands 1 and 2 (Table 3).

1) Band 1 (Figure 14b) is covered by infrared radiation. Lines are strongly absorbed (up to 85%), while only a fraction (<25%) of the continuum is absorbed.
2) Band 2 (Figure 14b) covers the visible light spectrum. Line emission and continuum behave similarly with up to 25% absorbed. Band 3 (Figure 14c) has negligible absorption (<3%) for continuum. Line absorption can be up to 30%.
3) Band 4 shows rapid absorption for line emission (>95%) while significant absorption of continuum up to 60% takes place over the temperature range from 3000 K to 5000 K (Figure 14c).
4) From band 5, line radiation becomes optically thick, completely absorbed within 0.0005 m. Over the longest optical path (Figure 14a),

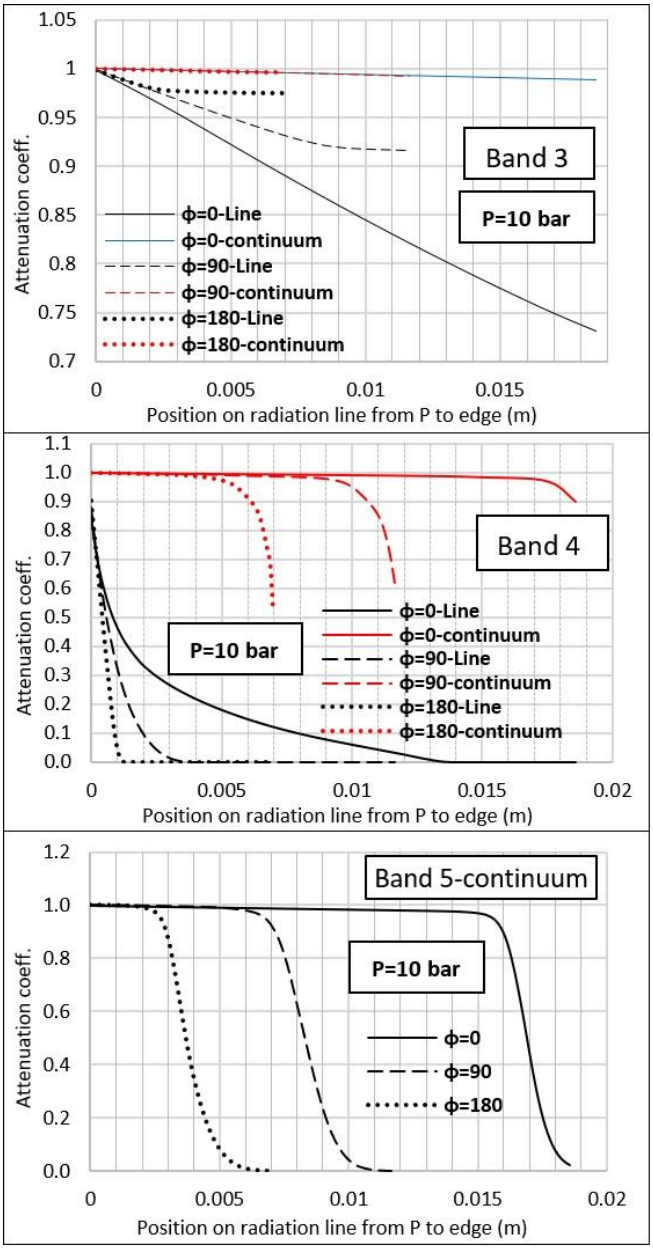

Figure 14c. Attenuation of 3 paths in Figure 14a in some typical frequencies of bands 3, 4 and 5 (Table 3).

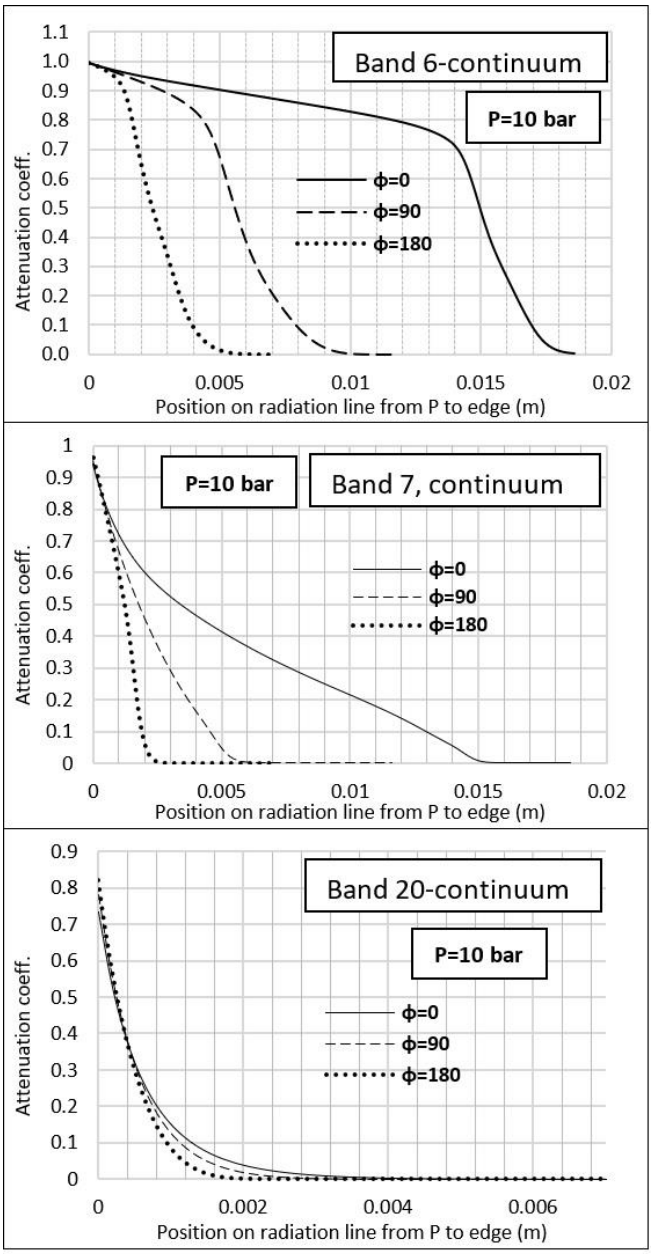

Figure 14d. Attenuation of 3 paths in Figure 14a in some typical frequencies of bands 6, 7 and 20 (Table 3).

continuum absorption gradually increases with increasing band number. 80% of the continuum absorption is reached at 5,000 K in band 6, 0.016 m away from point P. It is 22,000 K, in band 7, 0.01 m away from P; 0.003 m away from P in band 10, and 0.0007 m in band 20 (Figure 14d).

From the above observation, it becomes clear that photons with a frequency lower than 2×10^{15} Hz (150 nm in wavelength) can travel a considerable distance (> 0.02 m) with an attenuation factor of 0.2-0.8. Above 2×10^{15} Hz, only photons from the continuum spectrum can travel up to 0.015 m.

4.3 Spatial characteristics of radiation transfer in a typical cross-section of the arc column

The contribution to the radiative flux divergence at point P in Figure 2 from different directions, as defined by the polar angle (Θ) and azimuthal angle (φ), is also calculated. Based on conclusions at the end of Section 4.1, one polar angle (Θ=0, meaning in the target cross-section) and ten azimuthal directions have been chosen to focus on the contributions from different azimuthal directions. Radiative flux divergence is calculated based on the temperature profile of the middle cross-section in case A1, Table 2 (Temp 251). Figure 15a shows the ten directions on the radiation cross-section. The flux divergence is calculated for all the points from the arc's centre to edge (C to W in Figure 15a) in each direction, and results are displayed in Figures 15b, 15c, and 15d.

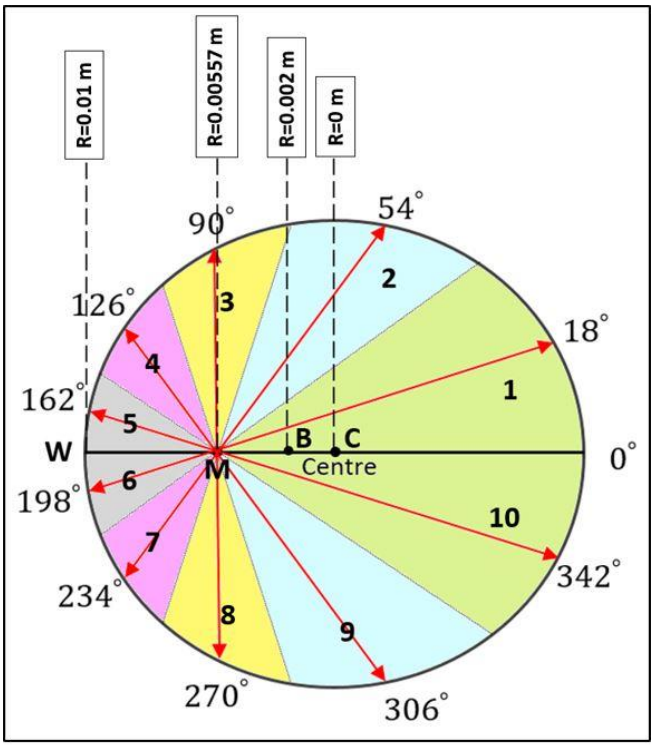

Figure 15a. A top view of the cross-section. M and B are the target points and red arrows are the lines of radiation propagation calculated. Each line covers one coloured area (areas 1 to 10).

Figures 15b and 15c show that directions close to φ=0 (or 360°) have a higher contribution to the absorption, and as φ moves toward 180 degrees, there is only emission loss from the point because its temperature becomes the highest in that direction. Almost all the absorption at point M (R=0.00557 m, net absorption peak in Figure 15d) comes from areas 1, 2, 9, and 10 in Figure 15a.

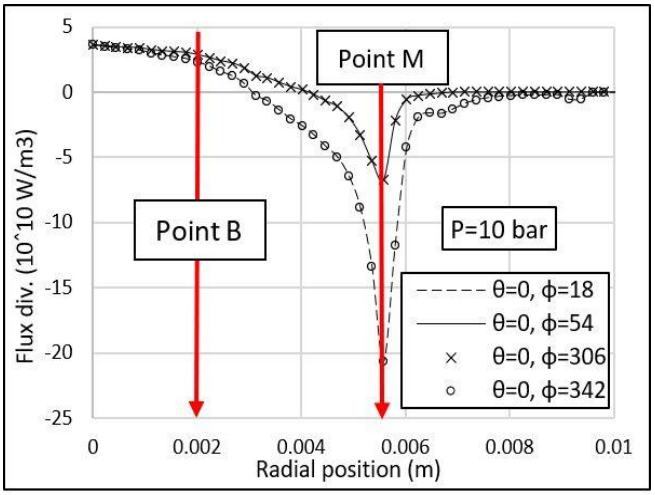

Figure 15b. Contribution of 4 different directions towards the radiative flux divergence at each radial position. Temp-251 in Figure 4 is used in calculation.

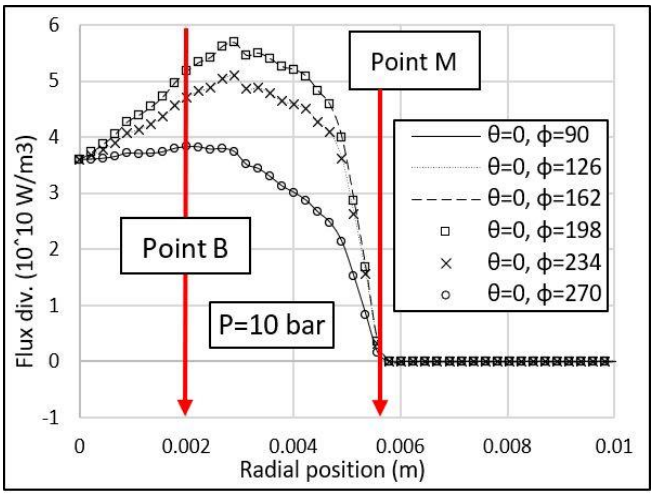

Figure 15c. Contribution of 6 different directions towards the radiative flux divergence at each radial position. Temp-251 in Figure 4 is used in calculation.

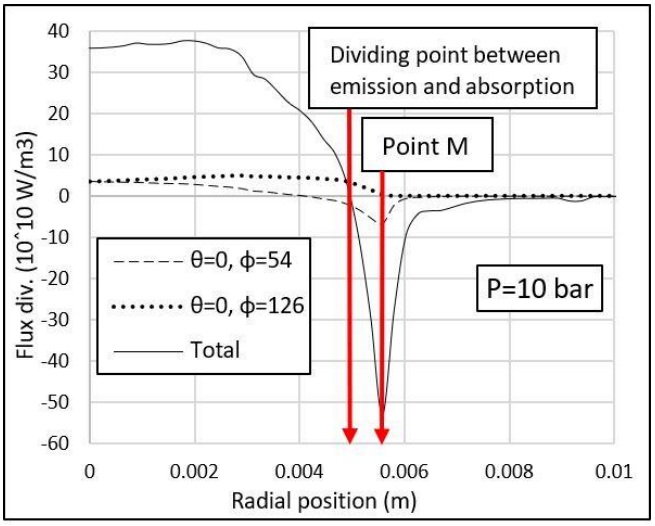

Figure 15d. Total radiative flux divergence at different radial positions and also the divergences contribution from two directions around ϕ=90.

At the centre of the arc, the contributions from different directions are similar due to axisymmetry. Moving toward the edge, the line of radiation propagation passing the vicinity of φ=0 (areas 1, 2, 9, 10) become longer. Those areas contain gases with a higher temperature than the target point. Thus, for target points far from the centre, such as point M as labelled in Figure 15b, where radiation absorption dominates, areas 1, 2, 9, and 10 are crucial (Figure 15b) while areas 3 to 8 make minimal contributions (Figure 15c) towards the total divergence because the gas temperature in these regions is not significantly higher than that at the target point.

Figure 15d shows the total radiative flux divergence (sum of all directions). The dividing point between the emission and absorption regions is the point of R=0.0047 m. Area 3 in Figure 15a (φ=90) separates areas 1 and 2 (radiation from these two areas is absorbed, see Figure 15b), from areas 4 and 5 (only emission loss from the target point, see Figure 15c). Radiative flux divergence of two of the mentioned areas is displayed in Figure 15d. Results here indicate that it is possible to use the divergence contributions from areas 2 and 4 only to estimate the location of this dividing point. The point with zero-sum is R=0.0049 m which is very close to the actual dividing point. Using R=0.0049 m can account for 98.5% of the actual absorption.

The percentage contribution of each direction to the total divergence at three typical radial positions are given in Figure 16. At the centre, the contribution from each direction is expected to be 10%, which is indeed the case. At point B (R=0.002 m), the net effect due to radiation transfer is emission. The maximum share is carried by the direction of φ=180, where the

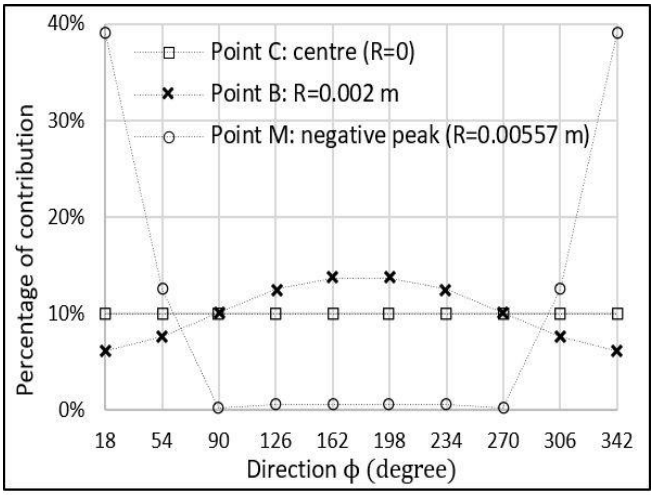

Figure 16. Contribution of each azimuthal direction (φ) to the total flux divergence at three typical radial positions.

temperature drops to the relatively lower environment temperature (around 3000 K) in the shortest distance. From Equation (5), the gradient of the Planck term (a function of temperature) determines the incremental effect over a temperature profile. At point M (R=0.00557 m, net absorption peak in Figure 15d), the net effect of radiation transfer is absorption. A detailed balance calculation shows that 99% of the radiative flux divergence is due to the contribution of areas 1, 2, 9, and 10, where the temperature of the gas is higher than point M.

5. Conclusions

The present work provides quantitative information on the spectral and spatial characteristics of radiation transfer, in an SF_6 arc column with uniform pressure. The temperature distribution is axisymmetric but varies along the axial direction. Although radiation transfer is an integral effect of spectral absorption coefficient that is a function of temperature and composition, the present work shows that photons with a frequency higher than 2×10^{15} Hz (shorter than 150 nm in wavelength) can hardly leave the central part of the arcing gas. Photons with a frequency of less than 1.5×10^{15} Hz (longer than 200 nm in wavelength) can escape the arcing gas in a significant proportion. The radiation escaping the arcing gas accounts for 25% to 45% of the net emitted energy from the arc centre.

For the 0.08 m long arc column, constructed from simulation results of an actual high-voltage circuit breaker with an instantaneous current of 15 kA, results show that it only needs to consider a slice of the column with a thickness of 0.024 m (0.012 m on each side of the target cross-section) to obtain an accuracy of better than 90% in the calculation of the radiative flux divergence, i.e. the net radiative power loss per unit volume at a point inside the arcing gas. About 55% - 75% of the radiation leaving the central high-temperature net emission core is trapped in the surrounding cooler zone. The exact percentage depends on the radial temperature profile.

Across a monotonic radial temperature distribution radiative energy is emitted from the central high-temperature core and partly absorbed at the arc edge. In the case of a thin slice of the column, i.e. over a cross-sectional area, whether a point emits or absorbs radiative energy depends on its location in the profile. When the emission from a point is lower than that from the arc centre, it experiences net radiation absorption. For the arc column under investigation, the net absorption zone starts at a point whose temperature is 75%-80% of the highest temperature at the centre. Using two directions on one side of a cross-section with axisymmetric temperature distribution is sufficient to determine the location of the starting point of the net absorption zone.

It is essential to adequately resolve the temperature variation over an optical path during the integration process; to correctly obtain the radiative flux divergence. An adaptive scheme for the spatial integration interval will effectively reduce the computing time. Information obtained from the present work is expected to help reduce the computational effort on integration, both in spectrum and space, to construct an approximate calculation method for engineering simulation of switching arcs.

Depending on the design of a circuit breaker, the arc at high current can burn in a mixture of SF_6 and PTFE vapour (in self-blast circuit breakers) or an SF_6 dominated environment (for puffer type circuit breakers). An SF_6 environment is chosen in this work because it is a simple yet representative situation that allows us to focus on the radiative characteristics of high current arcs. Adding PTFE vapour will severely complicate the study and make the results difficult to interpret. The radiation transfer phenomenon in high current self-blast arcs as well as in more environmentally friendly gases will be studied in the next stage of the investigation.

Acknowledgement

One of the authors (Esmaeili) would like to thank Hyosung Corporation for financial support during his PhD studies.

References

[1] R. Huang, H. Fukanuma, Y. Uesugi, Y. Tanaka, "An Improved Local Thermal Equilibrium Model of DC Arc Plasma Torch," IEEE Transactions on Plasma Science; Volume: 39, Issue: 10, pp. 1974 – 1982, 2011

[2] C. Mohsni, M. Baeva, St. Franke, et al., "Effect of a bidirectional coupling of an LTE arc column to a refractory cathode in atmospheric pressure argon," Phys. Plasmas 27, 073514 (2020)

[3] S. Tin, X. Zhang, Y. Cressault, et al., "Research status of replacement gases for SF6 in power industry," AIP Advances 10, 050702 (2020); doi: 10.1063/1.5134727, 2020

[4] M. Seeger, R. Smeets, J. Yan, et al., "Recent trends in development of high voltage circuit breakers with SF6 alternative gases," Plasma Physics and Technology, Vol. 4, No. 1 (2017), pp. 1-5, 2018

[5] Jeans, J. H. "The equations of radiative transfer of energy," Monthly Notices Royal Astronomical Society, vol. 78, pp. 28–36, 1917

[6] H. Nordborg and A. Iordanidis, "Self-consistent radiation-based modelling of electric arcs: I. efficient radiation approximations," J. Phys. D: Appl. Phys. 41, 135205, 2008
[7] H Z Randrianandraina, Y Cressault, A Gleizes, "Improvement of radiative transfer calculation for SF6 thermal plasmas," J. Phys. D: Appl. Phys. 44 (2011) 194012, 2011
[8] Michael F. Modest, "Radiation heat transfer," (3rd edition), Academic Press is an imprint of Elsevier, ISBN: 978-0-12-386944-9, chapter 16.1, pp.495, 2013
[9] Michael F. Modest, "Radiation heat transfer," (3rd edition), Academic Press is an imprint of Elsevier, ISBN: 978-0-12-386944-9, chapter 16.5, pp.507, 2013
[10] R I Soloukhin, "Radiative heat transfer in high-temperature gases (London: Hemisphere)," Chapters 3-6, 1987
[11] V. Aubrecht, E. T. Protasevich, "Radiative Transport of Energy in SF6 Arc Plasma," Manual of the Brno University of Technology and Tomsk Polytechnical University, pp. 42-46, 2000
[12] V Aubrechtt and J J Lowke, "Calculations of radiation transfer in SF6 plasmas using the method of partial characteristics," Journal of Physics D: Applied Physics 27, pp. 2066-2073, 1994
[13] JJ Lowke, J. Quant. Spectrosc. Radiat. Transfer 14, pp. 111-122, 1974
[14] J. Zhong, F. Yang, W. Wang, and J D. Yan, "Net Emission Coefficient and Radiation Transfer Characteristics of Thermal Plasma Generated in Nitrogen-PTFE Vapour Mixture," IEEE Transactions on plasma science, Digital Object Identifier: 10.1109/TPS.2018.2814399, 2018
[15] Y. Pei, J. Zhong, J. Zhang, and J. D. Yan, "A comparative study of arc behaviour in an auto-expansion circuit breaker with different arc durations," J. Phys. D: Appl. Phys., vol. 47, no. 33, pp. 335201, 2014.
[16] S. Chandrasekhar, "Radiative Transfer," Dover Publications, New York, 1960
[17] D. J. Hyde, J. S. Truelove, "The discrete ordinates approximation for multidimensional radiant heat transfer in furnaces," Technical Report VKAEA Report No. AERE-R 8502, Thermodynamics Division, AERE Harwell, Oxfordshire, 1977
[18] M. Seeger, L. Niemeyer, T. Christen, M. Schwinne, and R. Dommerque, "An integral arc model for ablation controlled arcs based on CFD simulations," J. Phys. D: Appl. Phys., vol. 39, no. 10, pp. 2180-2191, 2006
[19] Marc R.J. Charest, Clinton P.T. Groth, Ömer L. Gülder, "Solution of the equation of radiative transfer using a Newton–Krylov approach and adaptive mesh Refinement," Journal of Computational Physics 231, pp. 3023-3040, 2012
[20] Michael F. Modest, "Radiation heat transfer," (3rd edition), Academic Press is an imprint of Elsevier, ISBN: 978-0-12-386944-9, chapter 17.2, pp.544, 2013
[21] Michael F. Modest, "Radiation heat transfer," (3rd edition), Academic Press is an imprint of Elsevier, ISBN: 978-0-12-386944-9, chapter 15, pp.480-490, 2013
[22] H. C. Hottel and E. S. Cohen, "Radiant heat exchange in a gas-filled enclosure: Allowance for nonuniformity of gas temperature," AIChE Journal, vol. 4, pp. 3–14, 1958
[23] J. A. Fleck, "The calculation of nonlinear radiation transport by a Monte Carlo method: Statistical physics," Methods in Computational Physics, vol. 1, pp. 43–65, 1961
[24] Michael Eves, "Next Generation Network – SF6 Alternatives," Western Power Distribution, chapter 3.1, pp.11, 2018
[25] West, William, "Absorption of electromagnetic radiation," AccessScience, McGraw-Hill. Retrieved 8 April 2013
[26] Max Planck, "The Theory of Heat Radiation," Masius M. (transl.), (2nd ed.), chapter IV, pp. 168, 1914
[27] Michael F. Modest, "Radiation heat transfer," (3rd edition), Academic Press is an imprint of Elsevier, ISBN: 978-0-12-386944-9, chapter 10.4, pp.285, 2013
[28] W. Tiemann, "Spectroscopic temperature measurements of SF6 double nozzle arcs", Siemens Forsch. Entwickl. Ber., Vol. 14, pp. 317-324, 1985